

# Confinement approach to pressure effects on the dipole and the generalized oscillator strength of atomic hydrogen

R. Cabrera-Trujillo\*

*Instituto de Ciencias Físicas, Universidad Nacional Autónoma de México, Apartado Postal 48-3, Cuernavaca, Morelos 62251, Mexico and  
Departamento de Física, Universidad Autónoma Metropolitana-Iztapalapa, Apartado Postal 55-534, 09340, México, D.F., Mexico*

S. A. Cruz†

*Departamento de Física, Universidad Autónoma Metropolitana-Iztapalapa, Apartado Postal 55-534, 09340, México, D.F., Mexico*  
(Received 22 November 2012; published 9 January 2013)

Initial calculations to explore the role of pressure on generalized oscillator strengths (GOSs) for the hydrogen atom are presented. Our work is based on models of quantum confinement where the hydrogen atom is assumed to be spatially confined in a spherical cavity bounded by a barrier potential of finite height. For a given confinement radius and barrier height the energy spectrum for all available bound states and a number of continuum states (pseudocontinuum) is obtained by solving the Schrödinger equation using a finite-differences method. In contrast with the free atom case, the GOS momentum-transfer distribution for the  $1s \rightarrow nl$  transitions is enhanced in amplitude and width as pressure increases. A turnover of this behavior takes place at a critical pressure, indicating the approach to the limit of confining capacity for the system to hold the  $nl$  state. As a consequence of this behavior, the corresponding dipole oscillator strength (DOS) values provide a useful way to characterize the critical pressures for the fading and ultimate bleaching of the spectroscopic emission lines. It is also found that the height of the barrier—simulating different confining media—also affects these properties. These findings may be equally applicable to the study of inelastic energy loss from swift bare ions incident on matter under high pressures, photoabsorption, and photoionization cross sections of caged atoms as well as on optical properties of hydrogenic impurities trapped in spherical quantum dots.

DOI: [10.1103/PhysRevA.87.012502](https://doi.org/10.1103/PhysRevA.87.012502)

PACS number(s): 32.70.Cs, 62.50.-p, 37.30.+i, 31.15.xf

## I. INTRODUCTION

Any process of interaction of radiation with matter is fundamentally defined by the ability of the medium to absorb energy from the incident radiation (ions, electrons, or photons), which is intimately related to its electronic structure whether it is due to an aggregate of atoms or an isolated atom or molecule [1]. At the atomic level, the mechanisms of energy absorption depend on the allowed electronic transitions in the target atom consistent with the quantum-mechanical description of the target.

As originally pointed out by Bethe in his study of excitation and ionization cross sections for swift ion energy loss [2], the generalized oscillator strength (GOS) constitutes a measure of the bound-bound and bound-continuum transition probabilities for the electronic states of the target. This is a useful concept for the construction of the excitation function to account for the target energy absorption due to projectile momentum transfer [1]. This characteristic function not only pertains to ion-atom collision processes, but also to electron-atom collisions and photoionization processes [3–6]. In the limit of small momentum transfer,  $q \rightarrow 0$ , the function becomes the dipole oscillator strength (DOS) to account for dipole optical transitions. Therefore, knowledge of the GOS is not only of paramount importance in the study of radiation effects in matter but it is also important for understanding atomic spectroscopic properties.

To date, a great deal of knowledge has been accumulated on the properties of the GOS for free atomic and molecular

systems [1,3,4,7–10]. However, it is now well established that low-dimensionality materials have quite different electronic and optical properties as compared to their macroscopic counterparts [11]. This is also true for the behavior of atoms and molecules under high pressures as compared to their free condition [12,13]. Accordingly, the GOS (DOS) under such circumstances should be explored to develop a better understanding of energy absorption processes and spectroscopic properties of matter under nonconventional conditions.

The advent of new technologies for the synthesis of materials with low-dimensionality structures calls for the development of improved theoretical models to account for the electronic and optical properties of such systems. In this area, models of quantum confinement have proved to be appropriate (see Refs. [14–17] for a review).

With regard to the study of optical properties, recent years have seen an increasing interest in the use of confinement models to account for the behavior of dipole optical transitions—DOS—of low-dimensionality systems. One of the simplest and earliest examples where these ideas have been employed is that of color centers in alkali-metal halides [18], where one or two electrons are trapped in anion vacancy sites in the ionic lattice. More recently, the spectroscopic properties (DOS) of the hydrogen atom confined by hard [19–23] and soft [24] spherical cavities have been reported, as well as similar studies on the optical absorption of hydrogenic impurities in semiconductor quantum dots [25].

Recently, increasing attention has been focused on the study of photoionization cross sections of individual atoms inside endohedral fullerene cages for which giant resonances

\*trujillo@fis.unam.mx

†cruz@xanum.uam.mx

have been predicted [5,6,26] and observed [27]. Here, the GOSs play a major role and have been calculated through suitable confinement models. These findings motivated us to pursue—at the fundamental level—a systematic analysis of the GOS behavior for confinement conditions applicable to various physical situations such as the effect of pressure on the atomic excitation function.

The aim of this work is to present accurate calculations for the GOS of a hydrogen atom—as a basic reference system—confined by a penetrable spherical cavity of radius  $R_0$  and barrier height  $V_0$ , where  $V_0$  is assumed constant outside the confining cavity. In this context, different confinement radii and barrier heights correspond, respectively, to different pressures and host media. These two characteristics are not independent, since different host media provide different potential barrier heights which in turn—for a given cavity radius (pressure)—support different numbers of bound states. The assumption of a constant potential outside the confining region can be thought of as being produced by a metallic environment, since once the electron is out of the confinement region it does not feel the Coulomb attraction of the confined nucleus. However, this interpretation may also be assigned to an effective background constant potential due to the collective interactions with the medium, which is not necessarily metallic.

Although exact solutions for this Schrödinger problem exist [28,29], our aim here is to construct the whole energy spectrum through corresponding numerical solutions by means of a finite-differences approach. This is done for as many discrete states ( $E < V_0$ ) as can exist inside a confining box of radius  $R_0$  for a given barrier height  $V_0$ , as well as for a commensurable number of states ( $E \geq V_0$ ) in the continuum (pseudocontinuum). The corresponding wave functions, GOS, and DOS are calculated for different confinement conditions. Where available, our results are compared with other theoretical approaches.

Our work is organized as follows. In Sec. II, we provide an outline of the confinement model and the method followed to solve the time-independent Schrödinger equation by means of the finite-differences approach as well as its numerical implementation. In Sec. III, the results of this work together with their analysis and a discussion are presented. Finally, in Sec. IV, the general conclusions of this study are presented. Atomic units (energy in hartrees, length in bohrs) are used throughout unless otherwise specified.

## II. THEORETICAL APPROACH

We model the hydrogen atom under isotropic pressure by placing the atom inside a penetrable spherical confining box of radius  $R_0$ . We assume the nucleus is clamped at the center of the sphere and the electron is spatially limited within the confining box by a constant potential barrier of height  $V_0$  at the surface and outside of the cavity. Accordingly, our confining model potential is expressed as

$$V_c(r) = \begin{cases} -\frac{Z}{r}, & r < R_0, \\ V_0, & r \geq R_0, \end{cases} \quad (1)$$

where  $Z$  is the nuclear charge and  $r$  is the electron-nucleus separation.

Our first task is to find the electronic spectrum of the system under these confinement conditions. This requires solving the stationary one-electron Schrödinger equation associated with the potential function given by Eq. (1):

$$\left\{ -\frac{1}{2} \nabla^2 + V_c(r) \right\} \Psi = E \Psi. \quad (2)$$

Due to the spherical symmetry of the confining potential, we use spherical coordinates to simplify the three-dimensional Eq. (2). The radial and angular parts of this equation may be separated as usual so that the eigenfunctions of Eq. (2) become  $\Psi(r, \theta, \varphi) = R_{nl}(r) Y_l^m(\theta, \varphi)$ , where  $Y_l^m(\theta, \varphi)$  are the spherical harmonics associated to the orbital and magnetic quantum numbers  $l$  and  $m$ , respectively, and the functions  $R_{nl}(r)$  satisfy the radial equation

$$\left\{ -\frac{1}{2r^2} \frac{\partial}{\partial r} \left( r^2 \frac{\partial}{\partial r} \right) + \frac{l(l+1)}{2r^2} + V_c(r) \right\} R_{nl} = E R_{nl}. \quad (3)$$

This equation can be further simplified by making the change to  $u_{nl}(r) = r R_{nl}(r)$  obtaining

$$\left\{ -\frac{1}{2} \frac{\partial^2}{\partial r^2} + \frac{l(l+1)}{2r^2} + V_c(r) \right\} u_{nl} = E u_{nl} \quad (4)$$

which results in a one-dimensional self-adjoint equation for the radial variable.

In contrast with previous treatments of this problem, here we shall solve Eq. (4) numerically using the finite-differences approach which will be briefly described further below. An important characteristic of this method is that the only acceptable solutions are those consistent with the requirements  $u_{nl}(r = 0) = 0$ ,  $u_{nl}(r \rightarrow \infty) = 0$  and which connect smoothly at the boundary  $r = R_0$ . Accurate eigenvalues and eigenfunctions are found for several sets of confinement conditions ( $R_0$  and  $V_0$ ). An advantage of this method is that it can efficiently compute as many states as necessary both in the discrete as well as in the continuous spectrum (pseudocontinuum). This feature will prove to be very useful for the purposes of this work.

### A. Finite differences

We wish to find the eigenvalues and eigenvectors for each value of the angular momentum  $l$  and for each confining radius  $R_0$  and potential height  $V_0$  in Eq. (4). The finite-differences approach has been previously used in several time-dependent collision problems, e.g., wave-packet dynamics [30], transmission and reflection coefficients in quantum impurities [31], and charge transfer in atomic collisions under the influence of an ultrafast and strong laser pulse [32,33]. Thus, we will provide here only a brief sketch of the method. For further details, see Refs. [34,35].

We discretize the function  $u(x) \rightarrow u_k$  where  $x \rightarrow x_k$  is known at the  $k$ th point on a numerical grid. One type of computational grid consists of a set of fixed coordinate positions  $x_k$ , which may or may not be uniformly spaced. Thus,  $k = 0$  represents  $u_0$  and  $k = N + 1$  represents  $u_{N+1}$  which are the boundary conditions of the system, respectively, and thus

the wave function  $u_k$  is solved for  $k = \{1 \dots N\}$  points in the grid.

Equation (4) together with the boundary condition, which specify the value of  $u_0$  and  $u_{N+1}$ , can be written in matrix form by making a vector array  $\vec{u} = \{u_k\}$  and using the finite-differences definition for derivative and integration [34]. Thus

$$\mathbf{H}\vec{\varphi} = E\vec{\varphi}, \quad (5)$$

where  $\mathbf{H}$  is a tridiagonal matrix. The elements of  $\mathbf{H}$  are

$$\begin{aligned} H_{i,i} &= \frac{1}{2} \left[ \frac{1}{r_i - r_{i-1}} + \frac{1}{r_{i+1} - r_i} \right] \frac{1}{r_{i+1/2} - r_{i-1/2}} + V_i, \\ H_{i,i+1} &= -\frac{1}{2(r_{i+1} - r_i)} \frac{1}{\sqrt{(r_{i+1/2} - r_{i-1/2})(r_{i+3/2} - r_{i+1/2})}}, \\ H_{i,i-1} &= -\frac{1}{2(r_i - r_{i-1})} \frac{1}{\sqrt{(r_{i+1/2} - r_{i-1/2})(r_{i-1/2} - r_{i-3/2})}}, \end{aligned} \quad (6)$$

where  $V_i = \frac{l(l+1)}{2r_i^2} + V_c(r_i)$  and  $r_{i+1/2} = (r_{i+1} + r_i)/2$  defines the midpoint between two points in the grid. Here  $\vec{\varphi}$  is related to  $\vec{u}$  by means of  $\vec{\varphi} = \mathbf{L}^T \vec{u}$  where  $L_{ij} = \sqrt{r_{i+1/2} - r_{i-1/2}} \delta_{ij}$  is a diagonal matrix.

Equation (5) is just an eigenvalue problem in matrix algebra with the advantage of being a tridiagonal matrix which can be solved by LU decomposition [36]. The number of eigenvectors and eigenvalues thus depends on the number of grid points. One advantage of the finite-difference method is that the matrix  $\mathbf{H}$  includes the evaluation of the potential through the boundary  $r = R_0$  such that the eigenvalue solution also includes the correct behavior.

The only limitation of the finite-differences approach is the size of the numeric box, such that  $r \rightarrow \infty$  is replaced by  $r_{\max}$ . A suitable choice of  $r_{\max}$  renders as many states as required.

## B. Numerical implementation

The grid box we used to solve Eq. (5) extends from  $r = 0$  to  $r = 500$  with a total number of points  $N = 500$  spaced logarithmically in this range. Thus, the small increments are in the region of small  $r$ , providing a good cusp resolution on the wave function for  $r \rightarrow 0$ . This also provides a matrix of  $N \times N$  and  $N$  eigenvalues and eigenvectors. We note that in the finite-differences approach the precision requirements are controlled by  $\Delta r$  or by  $N$ , the number of points. The larger the number of points for the same range box, the better precision but larger matrices to invert.

The method has been implemented in a FORTRAN 95 code that generates the solutions and calculates the DOS and the GOS.

The eigenvectors and eigenvalues were obtained via tested LAPACK subroutines [37]. In a 2.8-GHz Pentium computer, a single  $R_0$  and  $V_0$  takes up to 120 min of CPU time.

## C. Elements of the generalized oscillator strength

As described in the Introduction, the excitation function for an atom to absorb energy from momentum transfer to its bound electrons is strongly defined by their probability to make a transition to a particular excited state. According to

Bethe [2], the GOS properly accounts for this probability and is defined as

$$F_{n0}(q) = \frac{2}{q^2} (E_n - E_0) |\langle \Psi_n | e^{i\mathbf{q}\cdot\mathbf{r}} | \Psi_0 \rangle|^2, \quad (7)$$

where  $\mathbf{q}$  is the momentum transfer,  $\Psi_n$  is the final excited state, and  $\Psi_0$  is the initial state from which the transition occurs. Additionally, after considering all possible excitations, the following relation—known as the Bethe sum rule (BSR) [1]—holds:

$$\sum_n F_{n0}(q) = N_e, \quad (8)$$

which is valid for any value of  $q$  and where the summation includes all discrete and continuum excited states and  $N_e$  is the number of bound electrons. The case  $q \rightarrow 0$  in Eq. (8) corresponds to the optical dipole oscillator strength which is the familiar Thomas-Reiche-Kuhn sum rule (TRK).

For our single electron problem under the previous assumptions, and considering the momentum transfer along the  $z$  axis, Eq. (7) becomes

$$F_{n0}(q) = \frac{2}{q^2} (E_n - E_0) |\langle n | e^{iqr \cos \theta} | 0 \rangle|^2 \quad (9)$$

where

$$\langle n | e^{iqr \cos \theta} | 0 \rangle = i^l \sqrt{2l+1} \int_0^\infty j_l(qr) u_{nl}^*(r) u_{10}(r) dr \quad (10)$$

with  $j_l$  the spherical Bessel function of order  $l$ . The integration is understood to be carried out only for the numerical radial wave functions  $u_{nl}$  complying with the boundary conditions, as prescribed by the finite-differences method. Note that we have chosen the ground state of the confined hydrogen atom ( $u_{10}$ ) as the initial state in Eq. (10). However, the same relation may be used for any other  $s$ -type initial state.

## III. RESULTS

### A. Bound energies

In order to test the accuracy of the finite-differences approach here proposed, we have calculated the energy dependence on cavity radius for the ground state and several excited states of the hydrogen atom for different values of the confining barrier height. Calculations were performed for several values of the confining radius  $R_0$  from 1.0 to 10 in steps of  $R_0 = 0.2$ . For the potential barrier heights we used the values of  $V_0 = 0, 0.1, 0.2, 0.5, 2.0, 5.0, 10.0, 50.0, 100$ , and  $V_0 = \infty$  (this last value is calculated by assuming numerically  $V_0 = 10^{300}$ ).

Figure 1(a) displays the energy behavior for the  $1s$ ,  $2s$ , and  $3s$  states as a function of  $R_0$  for a selected set of barrier heights:  $V_0 = 0$  (continuous line),  $V_0 = 2$  (long dashed line),  $V_0 = 10$  (short dashed line), and  $V_0 = \infty$  (dotted line). In the same figure, we compare our results with corresponding accurate calculations by Ley-Koo and Rubinstein [28] (open squares), Montgomery and Sen [24] (crosses), Goldman and Joslin [19] (open circles), and Laughlin [22] (plus signs). Also, for finite barrier heights, the critical cavity radius for which a given bound state exists is clearly observed at the leftmost side of each curve. The results of Montgomery and Sen [24]

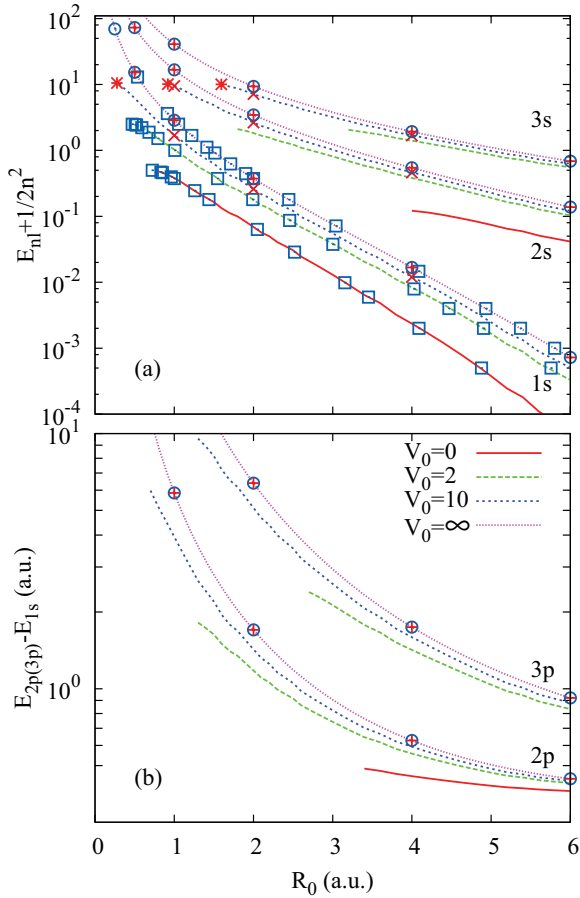


FIG. 1. (Color online) (a) Energy dependence on confinement radius ( $R_0$ ) and potential barrier height ( $V_0$ ) for the first three  $s$  states of the hydrogen atom. (b) Corresponding dependence for the  $1s \rightarrow 2p$  and  $1s \rightarrow 3p$  transition energies. Symbols represent accurate calculations available in the literature (see text): ( $\square$ ) Ley-Koo and Rubinstein [28]; ( $\times$ ) Montgomery and Sen [24]; (+) Laughlin [22]; ( $\circ$ ) Goldman and Joslin [19]. Note the critical radius for finite barrier heights below which the corresponding state is no longer bound. These values for  $V_0 = 10$  (\*) from Ref. [24] are shown for comparison.

( $V_0 = 10$ ) for these critical values are also shown (asterisks) for comparison. Our numerical values for both energies and critical radii correspond up to five decimal figures to those reported by the latter authors. Complementary to this figure, we show in Fig. 1(b) the energy difference between the  $1s$  and  $2p$  states and the  $1s$  and the  $3p$  states as a function of confinement radius for the same set of barrier heights. A blueshift of the associated optical transition, as the confinement radius is reduced, is apparent for all cases. This blueshift has already been predicted by Goldman and Joslin [19] for an infinite barrier potential. The open circles in this figure correspond to the transition energies reported by these authors as compared with the results of this work for a selected set of confinement radii. Also shown are the corresponding values reported by Laughlin [22] (plus signs).

As may be gathered from Figs. 1(a) and 1(b), the finite differences calculation gives excellent quantitative agreement with the other calculations, giving us confidence in the accuracy of our method. We can estimate the hydrostatic

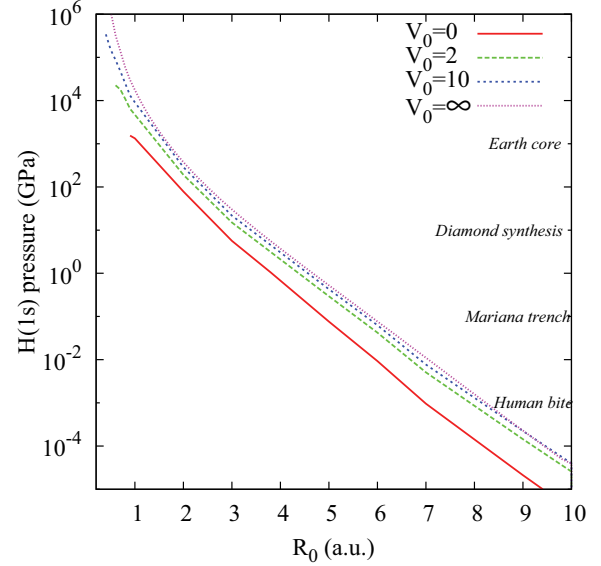


FIG. 2. (Color online) The computed atomic hydrogen pressure in GPa as a function of the cavity confinement radius  $R_0$  for different confinement potentials  $V_0$ . On the right are labeled some characteristic pressures that show some orders of magnitude.

pressure affecting the electronic system due to confinement effects in terms of the variations in the ground-state energy as the confinement volume changes, i.e.,

$$P_e = -\frac{\partial E_{1s}}{\partial V} = -\frac{1}{4\pi R_0^2} \left. \frac{dE_{1s}}{dR_0} \right|_{V_0}, \quad (11)$$

where  $V_0$  stands for the barrier height representing a particular environment.

In Fig. 2 we show the pressure in GPa as a function of the confining radius for the various potential barrier heights treated here. We note that the higher the potential barrier, the higher the confinement pressure for the same confinement radius. Note that below the critical radius for barrier heights  $V_0 = 0, 2$ , and  $10$  no bound state is available [see Fig. 1(a)] and hence the electron is no longer confined by the cavity. For  $R_0 \geq 2$ , a relative difference of about one order of magnitude for barriers within  $V_0 = 0$  and  $V_0 = \infty$  is observed for a given radius  $R_0$ . In the same figure, we show the order of magnitude of some characteristic pressures to give an idea of the ones we are dealing with. This figure will be useful as an aid to easily convert confinement radius to pressure units when discussing the associated behavior of the GOS and the DOS further below.

## B. Dipole oscillator strength

As pointed out in the Introduction, the DOS behavior of the confined hydrogen atom has been explored mainly through the infinitely hard spherical confinement model [19,21–23]. Only recently, Montgomery and Sen [24]—in their analysis of  $1s$  static and dynamic dipole polarizabilities—have reported calculations of the DOS sums equivalent to Eq. (8) for soft spherical confinement. In their calculation, the Bethe sum is truncated so as to include only all available  $1s \rightarrow np$  bound-bound transitions allowed by a confining potential of height  $V_0$ . They conclude that neglecting contributions from

the continuum brings the Bethe sum close to unity, hence this is a reasonable approximation.

We note here that—by construction—if  $N$  is the number of grid points, the finite-differences method used in this work allows us to obtain all  $N_B$  bound states for a particular value of  $R_0$  and  $V_0$  as well as the remaining states in the continuum. Of course, one would require an infinite number of grid points to include all the continuum states. However, we may call these unbound states a pseudocontinuum approximation enabling us to include these states in the Bethe sum.

Once the energy spectrum is obtained, together with the eigenfunctions, we can calculate the dipole oscillator strength for any allowed optical transitions  $nl \rightarrow n'l'$ . In particular, for the DOS calculation we must solve Eq. (4) for all states and substates with  $l = 0$  and  $l = 1$ . Since our interest here is to explore confinement effects on the DOS, we shall restrict ourselves to two specific calculations, namely for the  $1s \rightarrow 2p$  and  $1s \rightarrow 3p$  transitions.

Table I displays the individual DOS values obtained in this work for  $1s \rightarrow np$  ( $n = 2-5$ ) transitions for a selected set of confining barrier heights ( $V_0$ ) and radii ( $R_0$ ). We also include in this table corresponding accurate values reported in the literature for  $V_0 = \infty$  ( $R_0 = 1, 5, 10$ ) [22,23] and for  $V_0 = 100$  ( $R_0 = 1$ ) [24]. For these latter conditions, the results of this work show excellent quantitative agreement with those from the aforementioned independent calculations for all the DOS contributions. This allows us to gain confidence in the accuracy of the remaining DOS results for the other soft confinement conditions shown in this table, complementing the previous studies. In this connection, values for the TRK sum rule for all confinement conditions indicated in Table I are given in the last

row, where the only available calculations by Montgomery and Sen [24] for  $V_0 = 10$  ( $R_0 = 1, 5, 10$ ),  $V_0 = 100$  ( $R_0 = 1$ ), and  $V_0 = \infty$  ( $R_0 = 1, 10$ ) are included also for comparison. We note here that the TRK sums obtained in this work are closer to unity than those from the latter authors. This quantitative difference seems to arise from our inclusion of a higher number (500) of excited states in the calculation and considering the pseudocontinuum states.

We now turn our attention to the behavior of the DOS with changes in the degree of confinement. To this end, we have plotted in Figs. 3 and 4 the DOS dependence on  $R_0$  (pressure) for the  $1s \rightarrow 2p$  and  $1s \rightarrow 3p$  transitions, respectively, for different values of  $V_0$ .

We first observe from Fig. 3 that for the higher potential barriers ( $V_0 = 10, 100$ , and  $\infty$ ) the  $1s \rightarrow 2p$  DOS contribution increases as pressure increases (decreasing  $R_0$ ), reaching almost a value of unity for  $R_0 \sim 1$ . Also, for comparison purposes, the results for  $V_0 = \infty$  by Laughlin (crosses) [22] and Stevanović (open squares) [23] and the one for  $V_0 = 100$  by Montgomery and Sen (solid triangle) [24] are also shown for specific confinement radii. The free-atom DOS exact value  $f_{2p} = 0.416\,196\,0$  [39] for this transition (solid square) is also included as the limiting reference value for large values of  $R_0$  in our calculation. Excellent overall agreement is observed among all calculations (see further below). Note, however, that for the lower barrier heights ( $V_0 = 0$  and 2) a dramatic reduction of the DOS contribution takes place just before the critical radius is attained, at which point the excited state is no longer contained by the confining sphere and thus becomes part of the continuum. For the  $1s \rightarrow 3p$  transition, the DOS behavior is shown in Fig. 4. Again excellent overall agreement

TABLE I. Individual DOS contribution from  $1s \rightarrow np$  ( $n = 2-5$ ) transitions and TRK sum-rule values for a selected set of confinement radii and barrier height.

State	$V_0 = 0$			$V_0 = 2$			
	$R_0 = 1$	$R_0 = 5$	$R_0 = 10$	$R_0 = 1$	$R_0 = 5$	$R_0 = 10$	
$2p$		0.645413	0.440749		0.802359	0.475681	
$3p$			0.172295		0.139561	0.251260	
$4p$					0.003984	0.137730	
$5p$						0.065761	
TRK Sum	0.999919	0.999922	0.999923	0.999801	0.999918	0.999923	
State	$V_0 = 10$			$V_0 = 100$			
	$R_0 = 1$	$R_0 = 5$	$R_0 = 10$	$R_0 = 1$	$R_0 = 1$	$R_0 = 5$	$R_0 = 10$
$2p$	0.996363	0.827395	0.483303	0.985625 (0.986111) <sup>a</sup>	0.984553 (0.984558) <sup>b</sup> (0.984558) <sup>c</sup>	0.848786 (0.848799) <sup>b</sup> (0.846322) <sup>c</sup>	0.492028 (0.492039) <sup>b</sup> (0.492040) <sup>c</sup>
$3p$		0.123408	0.255048	0.006799 (0.006753) <sup>a,d</sup>	0.007725 (0.007726) <sup>b</sup>	0.108277 (0.108275) <sup>b</sup>	0.258159 (0.258174) <sup>b</sup>
$4p$		0.035764	0.134951	0.005761 (0.005788) <sup>a</sup>	0.005666 (0.005666) <sup>b</sup>	0.031944 (0.031942) <sup>b</sup>	0.131491 (0.131496) <sup>b</sup>
$5p$		0.007197	0.062813	0.000673 (0.000672) <sup>a</sup>	0.000744 (0.000742) <sup>b</sup>	0.005801 (0.005800) <sup>b</sup>	0.059562 (0.059561) <sup>b</sup>
TRK Sum	0.999673 (0.996623) <sup>a</sup>	0.999916	0.999923 (0.999199) <sup>a</sup>	0.999532 (0.999325) <sup>a</sup>	0.999993 (0.999983) <sup>a</sup>	0.999993	0.999988 (0.999813) <sup>a</sup>

<sup>a</sup>Values correspond to those reported by Montgomery and Sen [24].

<sup>b</sup>Values correspond to those reported by Stevanović [23].

<sup>c</sup>Values correspond to those reported by Laughlin [22].

<sup>d</sup>This is the correct value for the corresponding entry in Table 7 of Ref. [24] which was inadvertently inserted there as a typographic error [38].

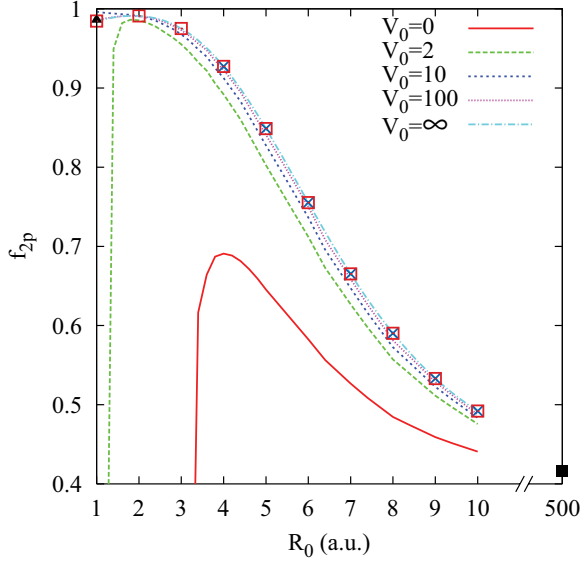


FIG. 3. (Color online) Dependence on confinement radius ( $R_0$ ) and potential barrier height ( $V_0$ ) of the dipole oscillator strength for the  $1s \rightarrow 2p$  transition in atomic hydrogen. Comparison is shown with accurate calculations: ( $\blacktriangle$ ) for  $V_0 = 100$  [24]; ( $\times$ ) [22] and ( $\square$ ) [23] for  $V_0 = \infty$ ; ( $\blacksquare$ ) free-atom case [39] (coincident with our calculation) (see text).

is observed with available calculations by Stevanović [23] for  $V_0 = \infty$  and with Montgomery and Sen [24] for  $V_0 = 100$  as well as with the corresponding free-atom DOS exact value  $f_{3p} = 0.079\,101\,6$  [39] for large  $R_0$ . Note, however, that the results shown in this figure for the  $1s \rightarrow 3p$  DOS dependence on pressure ( $R_0$ ) indicate a contrasting behavior as compared to the  $1s \rightarrow 2p$  transitions previously discussed. Namely, as pressure increases (decreasing  $R_0$ ) the  $1s \rightarrow 3p$  DOS contribution to the radiation intensity decreases and—except for  $V_0 = 0$ —a slightly larger DOS amplitude

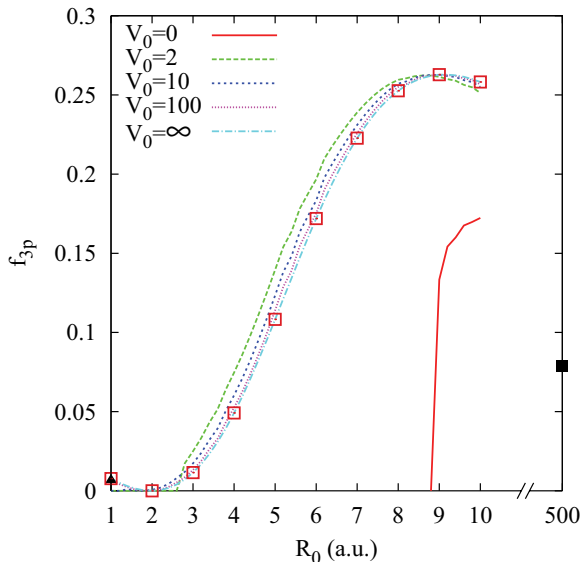


FIG. 4. (Color online) Same as in Fig. 3 for the  $1s \rightarrow 3p$  transition in atomic hydrogen.

is observed as  $V_0$  decreases (as long as it can still hold the bound  $3p$  state). The reasons for this behavior are still under study.

### C. Generalized oscillator strength

In contrast with the increasing number of DOS studies for the optical spectroscopic properties of the confined atom, the number of studies devoted to GOS properties is scarce. Analytical expressions for the free hydrogen atom GOS have been available in the literature for a long time [1,2,40]. The following analytical GOS expressions for a set of selected transitions for a free hydrogenlike atom of nuclear charge  $Z$  can serve as a reference in corresponding calculations for the confined system,

$1s \rightarrow 2s$ :

$$F_{2s}(q) = 24Z^{10} \frac{q^2}{(q^2 + (\frac{3Z}{2})^2)^6}, \quad (12)$$

$1s \rightarrow 2p$ :

$$F_{2p}(q) = 54Z^{12} \frac{1}{(q^2 + (\frac{3Z}{2})^2)^6}, \quad (13)$$

and  $1s \rightarrow 3p$ :

$$F_{3p}(q) = \frac{24}{9} Z^{12} \left( \frac{32\sqrt{6}}{81} \right)^2 \frac{(3q^2 + (\frac{4Z}{3})^2)^2}{(q^2 + (\frac{4Z}{3})^2)^8}. \quad (14)$$

We now focus our attention to the study of the GOS properties of the confined hydrogen atom treated so far. In contrast with the DOS calculation, for the GOS we require a high value for  $l$ , the angular momentum quantum number. We have calculated the GOS for values of the momentum transfer  $q$  up to 30 in steps of  $\Delta q = 0.1$  and we have found that a value of  $l$  up to  $l_{\max} = 100$  fulfills the Bethe sum rule up to five decimals.

Figures 5–7 show the GOS  $q$  dependence for the  $1s \rightarrow 2s$ ,  $2p$ , and  $3p$  transitions, respectively, for a selected set of confinement radii and keeping a fixed barrier potential height  $V_0 = 0$  as an example. For comparison, the corresponding free-atom GOS distributions according to Eqs. (12)–(14) are also shown in each case. We first note the excellent agreement between our numerical calculation for  $R_0 = 500$  (continuous curve) and the free atom analytical results in all cases (open circles) giving us confidence on the reliability of our GOS numerical calculation.

In all cases, both the height and width of the GOS distribution increase as the confinement radius decreases (increasing pressure). This behavior is in agreement with the Heisenberg uncertainty principle, since larger pressure means smaller confinement volume and therefore larger electronic momenta. Larger momentum transfer from the excitation source is thus required to produce a transition. This is more clearly evident for the  $1s \rightarrow 2s$  transition (Fig. 5), where a shift in the maximum of the distribution to higher momentum transfer is observed while in the optical threshold ( $q \rightarrow 0$ )  $F_{2s} \rightarrow f_{2s} = 0$  as expected, due to selection rules. Note, however, the dramatic reduction in the GOS amplitude for confinement radii close to the critical value for which the

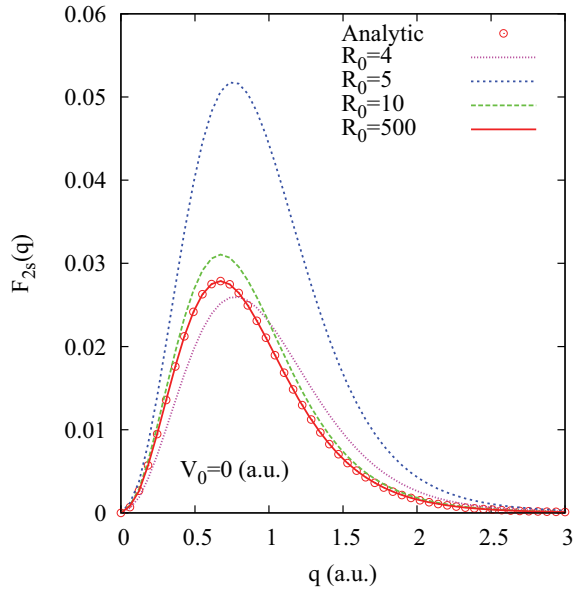


FIG. 5. (Color online) The generalized oscillator strength for the  $1s \rightarrow 2s$  transition for atomic hydrogen as a function of the momentum transfer  $q$  for several confinement radius  $R_0$  for the potential model with  $V_0 = 0$ . The circle symbols are the selected points from Eq. (12) the analytical expression for the free-atom case which shows good overall agreement with our selection  $R_0 = 500$  for this case.

excited transition state is still bound. Indeed, for  $V_0 = 0$  the critical radius holding the  $2s$  state is  $R_{2s} \sim 4$ , while for the  $2p$  and  $3p$  states the corresponding critical radii are  $R_{2p} \sim 3.3$  and  $R_{3p} \sim 8.8$ . The apparent GOS amplitude reduction observed in Figs. 5–7 for confinement radii close to these values points to an important critical property of the GOS—hence on the energy absorption function—imposed

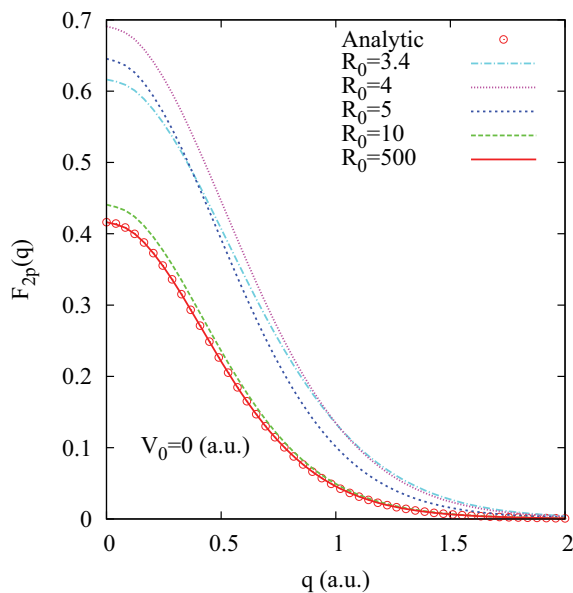


FIG. 6. (Color online) Same as in Fig. 5 for the  $1s \rightarrow 2p$  transition. The circle symbols are obtained from the analytic expression [Eq. (13)] for the free-atom case.

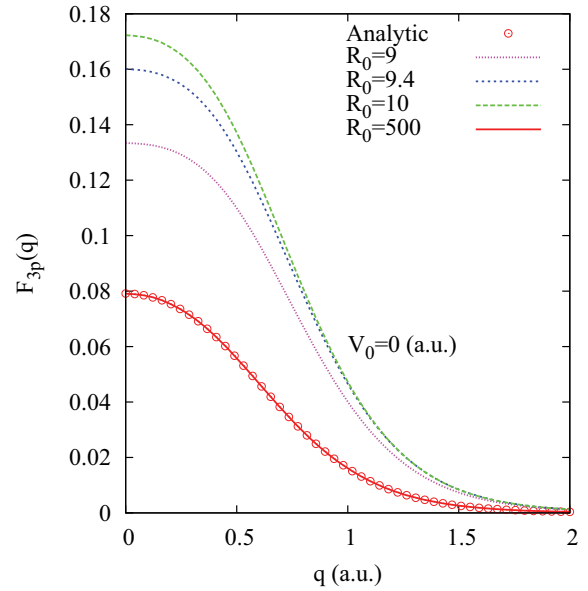


FIG. 7. (Color online) Same as in Fig. 5 for the  $1s \rightarrow 3p$  transition. The circle symbols are obtained from the analytic expression [Eq. (14)] for the free-atom case.

by the confining conditions. Close inspection of the excited-state wave-function behavior for the aforementioned critical confinement radii indicates a rapid reduction in amplitude as the critical confinement radius is approached. This behavior produces a reduced value in the transition matrix elements implied by Eq. (7) thus reducing the transition probability.

The consequences of this behavior on the DOS ( $q \rightarrow 0$ ) may be gathered from Figs. 6 and 7 for the  $1s \rightarrow 2p$ ,  $3p$  transitions, where a rapid increase in the DOS amplitude is observed for diminishing radius up to a value close to its critical value. At this point an important reduction takes place, ultimately disappearing for smaller confinement radii for which the excited state is no longer bound (see Figs. 3 and 4). Concerning pressure effects on observed optical transitions for the hydrogen atom, one would expect a blueshift as pressure increases with growing line brightness up to a pressure value where the line intensity diminishes until reaching a pressure for which the line disappears.

For numerical reference, Table II displays the GOS values calculated here for the  $1s \rightarrow 2s$ ,  $2p$ ,  $3s$ , and  $3p$  transitions for  $V_0 = 0$  in terms of the momentum transfer  $q$  and for a selected set of confinement radii  $R_0 = 5, 7$ , and  $10$ . In each case, the corresponding optical threshold (DOS) value ( $q \rightarrow 0$ ) is also shown complementary to Table I.

#### D. Dependence on the environment

Thus far, we have studied the GOS and the DOS behavior as a function of cavity size for a fixed confining barrier height. Since different barrier height values ( $V_0$ ) should represent different host media, clearly, the combined effect of cavity size and environment will ultimately define the behavior of these quantities. In this subsection we shall focus on exploring the influence of the height of the confining potential on the GOS distribution, keeping a fixed cavity size.

TABLE II. Generalized oscillator strength for the  $1s \rightarrow (2s, 2p, 3s, 3p)$  states of a confined hydrogen atom for a barrier height  $V_0 = 0$  and different confinement radii  $R_0$ .

$q$ (a.u.)	$V_0 = 0$							
	$R_0 = 5$		$R_0 = 7$		$R_0 = 10$			
	$F_{2s}$	$F_{2p}$	$F_{2s}$	$F_{2p}$	$F_{2s}$	$F_{3s}$	$F_{2p}$	$F_{3p}$
0.0	0.000000	0.645413	0.000000	0.526664	0.000000	0.000000	0.440749	0.172295
0.2	0.009697	0.595015	0.008899	0.478472	0.007287	0.001740	0.397154	0.168035
0.4	0.030736	0.468084	0.027179	0.361148	0.021605	0.006364	0.293435	0.151411
0.6	0.047608	0.317779	0.039752	0.230824	0.030375	0.011517	0.182622	0.119613
0.8	0.051555	0.189407	0.040135	0.128634	0.029495	0.014074	0.099411	0.080782
1.0	0.044342	0.101305	0.032122	0.064779	0.022894	0.013061	0.049266	0.047264
1.2	0.032480	0.049890	0.022103	0.030583	0.015439	0.009989	0.023035	0.024824
1.4	0.021267	0.023282	0.013837	0.013970	0.009548	0.006715	0.010455	0.012170
1.6	0.012932	0.010599	0.008201	0.006315	0.005615	0.004166	0.004704	0.005752
1.8	0.007537	0.004827	0.004724	0.002866	0.003217	0.002468	0.002128	0.002684
2.0	0.004315	0.002235	0.002689	0.001319	0.001825	0.001429	0.000978	0.001256

We show in Fig. 8 the GOS  $q$  dependence for a cavity radius of  $R_0 = 10$  for a set of potential barrier heights  $V_0$ . Even for this large cavity radius, a sensible shift in the GOS (and the DOS) amplitude is observed as the barrier height increases. For this cavity radius and the lowest barrier potential ( $V_0 = 0$ ) the estimated pressure corresponds to  $\sim 10$  Torr (or 0.01 atm) and yet the optical threshold DOS values between the free and confined case differ by about 5%. This difference increases as the confinement radius decreases (increment in pressure).

Varying the confinement barrier height (different host media) has a secondary effect on the GOS behavior, as compared with changes in cavity size. This may be verified by comparing the corresponding GOS amplitudes in Fig. 9

( $R_0 = 5$ ) and Fig. 8 ( $R_0 = 10$ ). Hence, compression plays a dominant role over the type of host medium.

**E. Bethe sum rule**

Finally, to assess the completeness of the numerical results reported so far, in Table III we show the values of the Bethe sum rule (BSR) [Eq. (8)] for a set of potential barrier heights and two values of the confinement radius  $R_0 = 5$  and 10 as a function of the momentum transfer  $q$ . First, we note that the higher the potential barrier, the closer to unity is the BSR. As the momentum transfer increases, the BSR deteriorates, resulting from higher angular momentum contributions. As Inokuti [1] has shown, the maximum of the GOS occurs when  $q_{\max}^2 \sim 2(E_n - E_0)$ , thus the larger the momentum transfer, the larger the number of  $n$  and  $l$  states is required to fulfill the BSR.

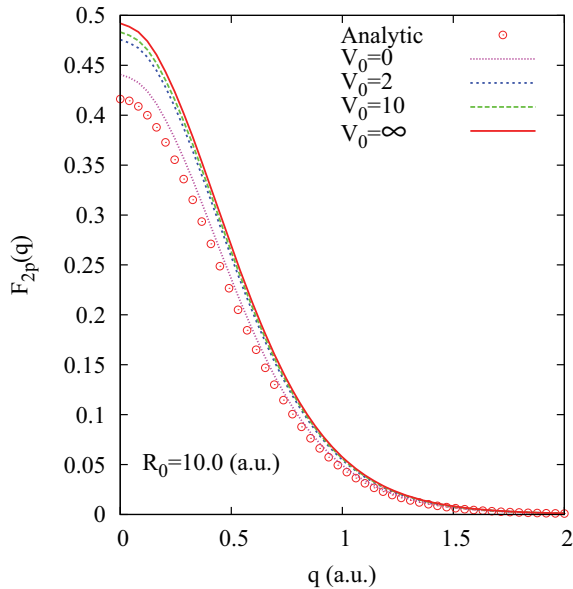


FIG. 8. (Color online) The generalized oscillator strength for the  $1s \rightarrow 2p$  transition dependence on momentum transfer  $q$  for atomic hydrogen confined in a spherical cavity with radius  $R_0 = 10$  and different potential barrier heights  $V_0$ . Circle symbols correspond to the free-atom case as in Fig. 6.

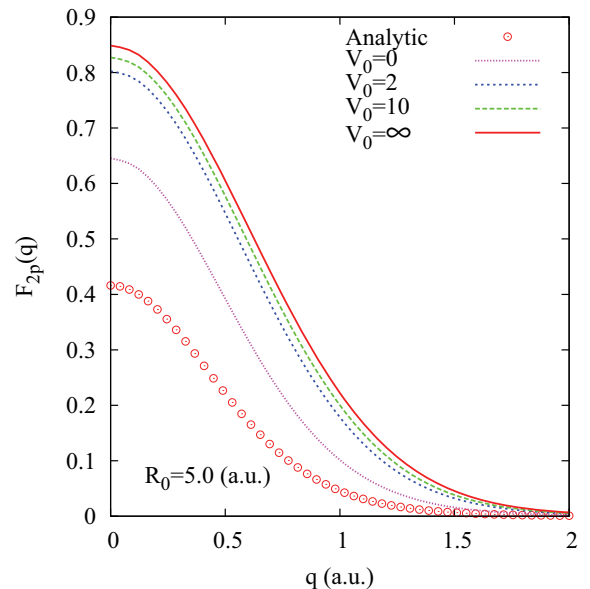


FIG. 9. (Color online) Same as in Fig. 8 for a confinement radius  $R_0 = 5$ .

TABLE III. Bethe sum rule as a function of the momentum transfer  $q$  for two confinement radii  $R_0$  and various barrier heights  $V_0$ .

$q$ (a.u.)	$V_0 = 0$		$V_0 = 2$		$V_0 = 10$		$V_0 = \infty$	
	$R_0 = 5$	$R_0 = 10$	$R_0 = 5$	$R_0 = 10$	$R_0 = 5$	$R_0 = 10$	$R_0 = 5$	$R_0 = 10$
0.0	0.999921	0.999923	0.999918	0.999923	0.999916	0.999923	0.999993	0.999988
0.1	0.999921	0.999923	0.999918	0.999923	0.999916	0.999923	0.999993	0.999988
0.2	0.999921	0.999922	0.999917	0.999922	0.999915	0.999922	0.999992	0.999988
0.5	0.999917	0.999918	0.999913	0.999918	0.999911	0.999918	0.999992	0.999987
1.0	0.999904	0.999905	0.999900	0.999905	0.999899	0.999905	0.999991	0.999986
2.0	0.999851	0.999851	0.999849	0.999851	0.999847	0.999851	0.999987	0.999978
4.0	0.999638	0.999635	0.999642	0.999635	0.999643	0.999636	0.999970	0.999946
6.0	0.999283	0.999277	0.999297	0.999277	0.999302	0.999277	0.999942	0.999892
8.0	0.998788	0.998776	0.998815	0.998777	0.998825	0.998777	0.999903	0.999817
10.0	0.998153	0.998134	0.998196	0.998134	0.998214	0.998134	0.999853	0.999721
20.0	0.992345	0.991867	0.993046	0.991869	0.993176	0.991871	0.999433	0.997936
30.0	0.969342	0.967588	0.973355	0.967592	0.975049	0.967594	0.990328	0.980706

IV. CONCLUSIONS

The role of spatial confinement on the atomic excitation function (GOS) and dipole (DOS) optical transitions for the hydrogen atom has been studied by considering the atom enclosed by a soft spherical cavity characterized by a radius  $R_0$  and an external step potential barrier of height  $V_0$  representing the confining capacity of the host medium for the atomic electron. The associated stationary Schrödinger problem was accurately solved using a finite-differences approach whereby the energy spectrum for bound and a commensurable number of continuum states (pseudocontinuum) were obtained, allowing for proper evaluation of GOS and DOS with close fulfillment of the corresponding Bethe and TRK sum rules for various confinement conditions.

It was found here that, as a consequence of confinement, the number of bound states for a particular barrier height is reduced as the confinement radius decreases, thus modifying the DOS and GOS intensities. In this connection, the GOS and DOS intensities monotonically increase as the confinement radius  $R_0$  decreases up to a fading point for  $R_0$  close to its critical value where the transition state is no longer bound. We believe this critical condition would represent the necessary pressure to stop observing a given transition line in optical

spectroscopy experiments. That is, the line would intensify as the pressure increases and then would fade until reaching the critical pressure for that line to disappear. Finally, the results of this work point to a predominance of cavity size (compression) effects over barrier height (host medium) on the GOS and the DOS behavior.

We believe that the approach here proposed may be an interesting alternative for studies where confinement effects on the atomic excitation function need to be accounted for, such as the study of inelastic energy loss processes arising from swift bare ions impinging on matter under high pressures, photoabsorption, and photoionization cross sections of caged-in atoms as well as optical properties of hydrogenic impurities trapped in spherical quantum dots.

ACKNOWLEDGMENTS

This work has been supported by PAPIIT-UNAM IN-101-611. We thank R. Garcia and the computer center at ICF-UNAM for technical support. We thank Professor L. Stevanović for providing us numerical values of her calculations and Professor H. E. Montgomery for useful comments on the manuscript. Finally, R.C.T. acknowledges UAM-I for the support and hospitality provided during his sabbatical stay.

[1] M. Inokuti, *Rev. Mod. Phys.* **43**, 297 (1971).  
 [2] H. A. Bethe, *Ann. Phys. (Leipzig)* **5**, 325 (1930).  
 [3] J. Botero and J. H. Macek, *Phys. Rev. A* **47**, 3413 (1993).  
 [4] Y. Fang, A. N. Vasil'ev, and V. V. Mikhailin, *Phys. Rev. A* **58**, 3683 (1998).  
 [5] M. Y. Amusia, L. V. Chernysheva, and E. Z. Liverts, *Int. J. Quantum Chem.* **112**, 3119 (2012).  
 [6] A. S. Baltenkov, V. K. Dolmatov, S. T. Manson, and A. Z. Msezane, *Phys. Rev. A* **79**, 043201 (2009).  
 [7] J. M. Peek and M. M. Madsen, *Phys. Rev. A* **43**, 147 (1991).  
 [8] M. A. Dillon, M. Inokuti, and Z. wen Wang, *Radiat. Res.* **102**, 151 (1985).  
 [9] R. A. Bonham, M. Inokuti, and R. S. Barbieri, *J. Phys. B* **26**, 3363 (1993).  
 [10] J. Wahedra and S. Khare, *Phys. Lett. A* **172**, 433 (1993).  
 [11] E. Degoli and S. Ossicini, in *Advances in Quantum Chemistry*, edited by J. Sabin and E. Brandas (Academic, New York, 2009), Vol. 58, pp. 203–279.  
 [12] R. F. W. Bader, in *Advances in Quantum Chemistry* Ref. [11], Vol. 57, pp. 285–318.  
 [13] D. Guerra, R. Vargas, P. Fuentealba, and J. Garza, in *Advances in Quantum Chemistry* Ref. [11], Vol. 58, pp. 1–12.  
 [14] W. Jaskólski, *Phys. Rep.* **271**, 1 (1996).  
 [15] J. P. Connerade, V. K. Dolmatov, and P. A. Lakshmi, *J. Phys. B* **33**, 251 (2000).

- [16] *Advances in Quantum Chemistry* Ref. [11], Vol. 57.
- [17] *Advances in Quantum Chemistry* Ref. [11], Vol. 58.
- [18] J. L. Marín, A. Clark, R. Rodríguez, R. Aceves, and S. A. Cruz, *J. Chem. Phys.* **76**, 3107 (1982).
- [19] S. Goldman and C. Joslin, *J. Phys. Chem.* **96**, 6021 (1992).
- [20] B. Saha, P. K. Mukherjee, and G. H. F. Diercksen, *Astron. Astrophys.* **396**, 337 (2002).
- [21] C. Laughlin, *J. Phys. B* **37**, 4085 (2004).
- [22] C. Laughlin, in *Advances in Quantum Chemistry*, edited by J. R. Sabin and E. Brandas (Academic, New York, 2009), Vol. 57, pp. 203–239.
- [23] L. Stevanović, *J. Phys. B* **43**, 165002 (2010).
- [24] H. E. Montgomery and K. D. Sen, *Phys. Lett. A* **376**, 1992 (2012).
- [25] S. J. Liang and W. F. Xie, *Eur. Phys. J. B* **81**, 79 (2011).
- [26] V. K. Dolmatov, J. L. King, and J. C. Oglesby, *J. Phys. B* **45**, 105102 (2012).
- [27] A. L. D. Kilcoyne, A. Aguilar, A. Müller, S. Schippers, C. Cisneros, G. Alna'Washi, N. B. Aryal, K. K. Baral, D. A. Esteves, C. M. Thomas, and R. A. Phaneuf, *Phys. Rev. Lett.* **105**, 213001 (2010).
- [28] E. Ley-Koo and S. Rubinstein, *J. Chem. Phys.* **71**, 351 (1979).
- [29] N. Aquino, G. Campoy, and H. E. Montgomery, *Int. J. Quantum Chem.* **107**, 1548 (2007).
- [30] A. Goldberg, H. M. Schey, and J. L. Schwartz, *Am. J. Phys.* **35**, 177 (1967).
- [31] R. Cabrera-Trujillo and F. J. Domínguez-Gutiérrez, *Radiat. Eff. Defects Solids* **167**, 464 (2012).
- [32] F. Anis, V. Roudnev, R. Cabrera-Trujillo, and B. D. Esry, *Phys. Rev. A* **73**, 043414 (2006).
- [33] R. Cabrera-Trujillo, J. I. Jiménez-Mier, and A. M. Juárez, in *Femtosecond-Scale Optics*, edited by A. V. Andreev (InTech, Rijeka, Croatia, 2011), pp. 169–202.
- [34] S. E. Kooning and D. C. Meredith, *Computational Physics, FORTRAN version* (Perseus, Reading, MA, 1990).
- [35] M. W. J. Bromley and B. D. Esry, *Phys. Rev. A* **69**, 053620 (2004).
- [36] W. H. Press, S. A. Teukolsky, W. T. Vetterling, and B. P. Flannery, *Numerical Recipes*, 2nd ed. (Cambridge University Press, New York, 1992).
- [37] E. Anderson, Z. Bai, C. Bischof, S. Blackford, J. Demmel, J. Dongarra, J. Du Croz, A. Greenbaum, S. Hammarling, A. McKenney, and D. Sorensen, *LAPACK Users' Guide*, 3rd ed. (Society for Industrial and Applied Mathematics, Philadelphia, 1999).
- [38] H. E. Montgomery (private communication).
- [39] H. C. Goldwire, *Astrophys. J. Supl.* **17**, 445 (1968).
- [40] N. F. Mott and H. S. W. Massey, *The Theory of Atomic Collisions*, 3rd ed. (Clarendon, Oxford, 1965).